JTTEE5 7:383-391

PEER REVIEWED

Analysis of the Nonthermal Emission Signal Present in a Molybdenum Particle-Laden Plasma-Spray Plume

K. Hollis and R. Neiser

(Submitted 2 January 1998; in revised form 17 March 1998)

In-flight measurement of the surface temperature of plasma-sprayed particles is important for the correlation of particle characteristics to coating structure and properties. However, the use of optical pyrometry for particle surface temperature measurement has inherent uncertainties due to nonthermal emission signals in the plasma/particle plume. This nonthermal signal is especially bothersome near the torch exit and in regions of the plume where there are few particles. This work presents measurements of the nonthermal signals present when making temperature measurements of plasma-sprayed molybdenum particles. Changes in the nonthermal emission signals were found to be caused by particle vapor, the spectral plasma loading effect, and particle reflection of plasma light. Care must be taken to avoid particle temperature errors due to these effects.

Keywords diagnostic, line emission, nonthermal correction, particle pyrometry

1. Introduction

The temperature of plasma-sprayed particles is an important parameter to be measured for better understanding of the plasma-spraying process. Particle temperature has been shown to be an important parameter in predicting particle flattening (Ref 1) and is thought to play a major role in coating formation (Ref 2). An accurate measurement of particle temperature is needed in order to determine a reliable correlation between in-flight particle temperatures, and coating structure and properties. In order to model the plasma-spray process, an understanding of heat transfer between the plasma and the particles is necessary to improve the accuracy of plasma-particle interaction modeling. Thus, an accurate measure of particle temperature in flight will help in understanding the phenomena before and after impact of the particle against the substrate.

The measurement of particle temperature by optical pyrometry has been accomplished by researchers using various methods. For example, see Ref 3 to 5. Inherent in the optical pyrometric method are sources of error in the temperature calculation. The error arises from the collection and analysis of the optical emission signal. Along with the particle thermal emission signal, other "nonthermal" emission signals are collected. Failure to identify and remove the nonthermal signals leads to errors in calculating particle surface temperatures (Ref 6, 7). The effect of nonthermal signals is especially large near the plasma torch exit or in regions where there are few or relatively cool particles. Therefore, it is necessary to identify the nonthermal signals and to devise a way of subtracting them from the collected optical signals used for particle pyrometry, in order to improve particle surface temperature measurements.

The work presented here describes a method for identifying and quantifying the nonthermal signals present in the spectra collected. Molybdenum particles in an argon-helium plasma were investigated. The method involves the quantification of particle masking, the optical plasma loading effect, and the particle-reflected plasma light signal. In addition, the particle vapor signal was analyzed to determine the species composition and the line emission behavior of the radiating vapor. The measurements helped define a method for subtracting the nonthermal signals from the raw data, which improved the accuracy of particle temperature calculations. This subtraction method is presented in an accompanying paper (Ref 6).

K. Hollis, Los Alamos National Laboratory, MST-6 Metallurgy, MS G-770, PO Box 1663, Los Alamos, NM 87545, USA; and **R. Neiser,** Sandia National Laboratory, Albuquerque, NM. Contact e-mail: khollis@lanl.gov.

2. Background

An optical pyrometer uses measurement of the thermal radiation emitted from an object to determine the temperature of the surface of that object. The relation between the spectral thermal emission and the temperature of a particle is determined by the specific thermal radiative properties of the material and the laws of thermal radiation heat transfer. The spectral or wavelength distribution of the emitted thermal flux is given by the Planck equation

$$M_\lambda = \varepsilon(T,\lambda)c_1\lambda^{-5}[\exp(c_2/\lambda T) - 1]^{-1} \quad \text{(Eq 1)}$$

where M_λ is the spectral thermal emission intensity, c_1 is the first radiation constant, c_2 is the second radiation constant, λ is the wavelength of the radiation, T is the absolute surface temperature, and $\varepsilon(T,\lambda)$ is the proportionality factor for non-blackbodies known as the emittance, which is a function of wavelength and temperature. Collecting the emitted thermal radiation at a known wavelength from a particle with a known emittance

allows for the calculation of the particle surface temperature from the Planck equation.

When collecting the thermal emission signal from particles in a plasma plume, several nonthermal signals are also collected, including:

- The line and continuum emission from the plasma surrounding the particles in the optical detector sampling volume
- The line and continuum emission from the intensely bright arc and plasma in the throat of the gun which is reflected into the detector by the particles that act as radiation scatterers
- The line and continuum emission from the vaporized particle material that is spread throughout the plume

Several authors have pointed out that the primary limitation in measuring particle thermal emission is the presence of the bright plasma near the exit of the plasma torch (Ref 3-5). Sakuta and Boulos (Ref 8) have calculated the relative intensities of plasma and particle emission in the detector field of view, in an effort to determine where the plasma signal drowns out the particle thermal emission. Gougeon and Moreau (Ref 9) have calculated the amount of particle-reflected plasma light that is collected with the thermal emission. Their calculations showed that the particle-reflected radiation can represent a significant source of temperature calculation error. The smaller, cooler, and closer to the torch exit plane the particle is, the more significant the error. However, from a simulated particle radiation reflection measurement, Prucha and Skarda (Ref 10) concluded that the plasma light scattered by the particles does not need to be considered for in-flight particle pyrometry. Clearly, more accurate measurement of the nonthermal signals present will help to better understand the limitations of in-flight particle pyrometry. Furthermore, if nonthermal signals can be subtracted from the raw collected signals, more accurate temperature measurements can be made.

There are several sources of nonthermal line and continuum radiation in the particle-laden plasma plume. One is the plasma itself. The gases used for the primary, secondary, and powder-carrier gases are heated by the electric arc in the torch, and emit line and continuum radiation. Another source of radiation is the vapor produced by the vaporization of the outer surface of particles in the hot plasma. Due to collisions with the hot plasma gases or the absorption of radiation from the plasma arc, energy is imparted to the vapor released from the particles. The excited vapor atoms then spontaneously decay to a lower energy state, producing characteristic radiation.

For particle pyrometry measurements, it is necessary to know what nonthermal radiation signals are present in addition to the thermal emission from the particle surface, in order to make accurate particle temperature measurements. Two spectral signal measurements that can be made perpendicular to the trajectory of the plasma and particles are: the signal with the plasma only (particle feed off), and the signal with the plasma and particles (particle feed on). When particles are added to the plasma, changes in the emitted radiation spectrum result. The changes are due to thermal radiation from the particle surface, particle vapor radiation, particle masking of the plasma radiation, the spectral plasma loading effect, and the particle-reflected plasma signal.

The particle-masking effect occurs as particles pass through the collection volume of the detector. The light behind the particles, either from the thermal emission of other particles or from nonthermal emission, is blocked from the detector by the opaque particle. Therefore, the radiation signal detected is reduced in proportion to the number and size of masking particles in the detection volume.

The spectral plasma loading effect occurs when particles are introduced into the plasma. The plasma emission is decreased by two mechanisms. The first is from particles absorbing energy from the plasma by heat transfer. The decrease in plasma kinetic energy causes a subsequent decrease in plasma emission. The second mechanism whereby the spectral plasma loading effect modifies the collected radiation spectra is vapor absorption. The vapor which emanates from the rapidly heated particle surface absorbs some of the plasma radiation, thereby attenuating the plasma emission signal.

A third effect that modifies the collected spectra is particle-reflected plasma radiation. As the particles pass through the detector collection volume, they act as scattering points for radiation traveling in the same direction as the particles ("head-on" radiation). The source of this radiation is primarily the intensely bright plasma arc struck between the anode and cathode in the plasma torch. The anode acts to reflect the arc radiation preferentially in the direction of the exiting plasma. The particle surface reflects the light from the arc through a 90° angle to the detector. In this way, light from the arc that is not detected without particles in the detection volume is detected when particles are present and act as scattering centers. So, by the particle-reflected plasma radiation effect, the collected spectra are increased in intensity by the additional plasma radiation.

3. Data Collection

The plasma torch used for this experiment is the commercially available Miller Thermal, Inc. SG-100 (Miller Thermal Inc., Appleton, WI). The torch parameters used are listed in Table 1. The powder used was Miller Thermal AI-1013 (Miller Thermal Inc., Appleton, WI) molybdenum which was cut to a 63 to 75 μm diameter size distribution. The powder feed rate was a relatively low 10 g/min. Spraying was carried out in the local atmospheric pressure of 90 kPa. The argon and helium used were standard industrial grade with a purity of 99.995%.

In order to gain an understanding of the various sources of radiation present in the plasma-particle plume, optical sampling must take place over a broad spectral range with sufficient precision within the range to identify characteristic line emission.

Table 1 SG-100 torch parameters

Parameter	Value
Torch current	795 A
Torch voltage	36.6 V
Ar arc gas flow rate	40.1 slm(a)
He arc gas flow rate	24.1 slm(a)
Ar powder gas flow rate	3.8 slm(a)
Anode/cathode/gas injector	720/730/112(b)

(a) Standard liters per minute. (b) Miller Thermal, Inc., part numbers

For this investigation, radiation in the range of 340 to 880 nm, with an intensity reading every 0.36 nm, was sampled. Quickly collecting data over such a range necessitates the use of multiple detectors. Here, a model TN-6132 intensified 1024 element linear diode array detector (Tracor Northern, Middleton, WI) was used for data collection. However, the low sensitivity of the diodes precluded the resolution of single-particle emission spectra. So, the emission from many particles passing through the sampling volume was recorded for each location in the plume. Thus, the method of optical sampling used for this investigation is best described as multicolor, multiparticle. The method is similar to that used by Kuroda et al. (Ref 4).

The optical sampling equipment setup is shown in Fig. 1. The light shield, light trap, and tubes covering the optic path were used to reduce detection of room reflected light. The optical detection system chosen for this experiment was a 1/3 m focal length spectrograph with an intensified 1024 element linear diode array. The sensitive range of the intensifier/detector combination was from 300 to 900 nm. The signals from the diodes were fed into a detector controller and then into a personal computer for storage. The collection lens was a 209 mm, f/4.5 photographic lens. The light passed from the lens through a cutoff filter before entering the spectrograph. The cutoff filter was used to eliminate second order wavelength light detection. Resolution of the spectra was controlled by the 250 μm horizontal entrance slit to the spectrograph. The measurement volume was approximately 25 μm high by 250 μm wide by 2 cm deep. When recording spectra, five exposures were taken sequentially and averaged. This averaged data was used for all subsequent analysis.

The diode signals were calibrated for wavelength using calibration lamps which provide line emission at known wavelengths. The diode-to-wavelength calibration was determined by fitting a quadratic formula to the diode number and known wavelength information. The spectral sensitivity was determined using a tungsten strip lamp traceable to a National Institute of Standards and Technology calibration. The temperature of the lamp was known for a given lamp current. Using the spectral emittance for the tungsten strip and Planck's relation for the spectral radiation emitted from a blackbody at a known temperature, the instrument response function (IRF) for the optical components and the detection system was determined.

The spatial data sampling coordinates are shown in Fig. 2. Data were taken between $x = 50$ and 200 mm. Spectra were recorded at y-coordinate increments of 1.09 mm. Two types of spectra were recorded. The first type of spectrum was recorded with particles in the plasma and is referred to as a "with-particle" spectrum. The next type of spectrum was recorded at the same locations as the with-particle spectrum but no particles were injected into the plasma during data collection. This type of spectrum is called a "without-particle" spectrum.

4. Analysis and Discussion

The first step in the analysis of the collected spectra is to subtract the detector dark current. Next, the IRF determined previously is used to correct the spectra for the combined spectral response of the optical detection system. Since the integration time of the detector was varied based on the intensity of the collected signal, the data were corrected for the same effective integration time. Therefore, the intensities of the corrected spectra can be compared to each other on an accurate relative basis. Since the plasma is assumed to be nonoptically dense in the region sampled, self-absorption effects are neglected.

4.1 Line Identification

Characteristic line emission analysis of the with-particle data was performed to identify the dominant lines in the collected signal in the 340 to 880 nm spectral range. The lines present were identified as originating from molybdenum, chromium, argon, sodium, and potassium. Reference 11 was used for atomic line emission identification. These lines can be seen for the spectra collected at $x = 50$ mm, $y = 0$ mm in Fig. 3. The chromium is a likely impurity in the molybdenum powder owing to its chemical similarity. The source of the sodium and potassium is unknown, but even small quantities of these elements can be observed due to their very strong emission lines. The relative intensity of the emission lines from the different emitting species varies as a function of position in the plume. Therefore, the line radiation spectrum contains strong emission from the vapor of the main powder component (molybdenum), several powder impurity substances (chromium, sodium, and potassium), and the expected line radiation from the plasma gas (argon). Note that in addition to the line emission evident in the spectra, there

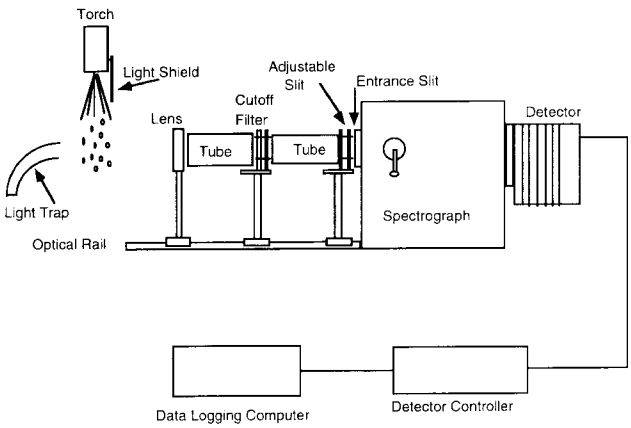

Fig. 1 Experimental setup for optical sampling

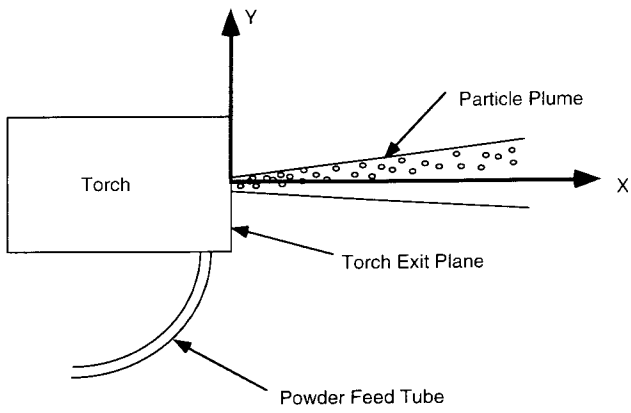

Fig. 2 Axes for spectral measurements

is also some contribution to the continuum radiation from the species identified above.

4.2 Molybdenum and Sodium Line Analysis

Further investigation of the vapor line signals present in the collected spectra reveals important aspects of the line intensity variation which should be considered when attempting particle temperature measurements. Figures 4 to 7 show the line intensity for the molybdenum line at 379.8 nm and the unresolved sodium doublet at 589.0 and 589.6 nm. Figure 8 shows the line intensity for all y-positions added together as a function of x-distance for the molybdenum and sodium lines. The intensity of the molybdenum line drops drastically from $x = 50$ to 80 mm and then decays more slowly from 80 to 140 mm. The sodium line intensity, however, drops evenly from 50 to 140 mm with a very nearly exponential decay, as seen on the semi-log plot. The line intensity decreases are due to a combination of the decrease in available exciter energy and the decrease in vapor concentration.

Note, too, the location of maximum intensity for a given x-location for the molydenum and sodium lines. At $x = 50$ mm (Fig. 4), both line intensity distributions are peaked at about $y = 3$ mm. However, at $x = 80$ mm (Fig. 5), the sodium intensity distribution is still peaked at about $y = 3$ mm but is no longer symmetric and falls off more slowly for more positive values of the y-coordinate. The intensity distribution of the molybdenum line is still fairly symmetric but is now peaked at about $y = 8$ mm. This trend continues at $x = 110$ mm (Fig. 6) where the sodium line intensity distribution is broad, with high values stretching from $y = 0$ to 10 mm. By contrast, the molybdenum line intensity distribution is much narrower and peaked at $y = 10$ mm. However, at $x = 140$ mm (Fig. 7), both the molybdenum and the sodium line intensity distributions look very similar in shape. The similarity in distributions continues to $x = 200$ mm after which the line emission is much less than the thermal emission and is difficult to accurately quantify.

Because the intensity of line emission for a given vapor depends primarily on the amount of vapor present and the availability of excitation energy, the variation in line intensity distributions for the molybdenum and sodium lines can be explained. As the x-distance from the energy source, the plasma arc, increases, the amount of energy available for excitation decreases. As seen in Fig. 8, there is a significant difference in the rate of decrease of the intensity of the molybdenum and the sodium lines. Because the excitation energy source for the two vapors decreases with x-distance in the same way, the difference in the rate of intensity decay must be due to a more rapid decrease in the concentration of molybdenum vapor than of the sodium vapor. Thus, the large drop in the intensity of the molybdenum line is most likely due to a large decrease in the rate of vaporization of the molybdenum particles after they leave the hot plasma. The decrease in vaporization causes a decrease in the local concentration of molybdenum vapor, thus decreasing the molybdenum line radiation. This shows that molybdenum line emission is primarily vapor-concentration limited in the range investigated.

The difference in the shapes of the emission line intensity distributions for the two vapors for a given x-position can also be explained in terms of the excitation energy and the vapor concentrations present. The molybdenum line intensity distribution is very similar in shape and position to the hot particle distribution. This can be seen by comparing the molybdenum line intensity to the hot particle flux distributions in Fig. 5 to 7. An accompanying paper gives a detailed description of the hot particle flux measurements (Ref 6). The similarity in location of the molybdenum line intensity distribution and the molybdenum particle number distribution indicates that the molybdenum line emission is strongly dependent on the particle flux, which in turn determines local vapor concentrations. As the surface of the particles vaporizes, the concentration of vapor around the particles is high. Away from the particles, the vapor concentration is lower, due to a dilution of the vapor. The areas of lower vapor concentration also have lower molybdenum line emission. This does not appear to be the case for the sodium lines, however, until $x = 140$ mm and beyond. At $x = 80$ mm and $x = 110$ mm, the sodium line intensity is strong near the $y = 0$ mm position, even though the particles are moving away from the $y = 0$ mm torch centerline. This is likely due to the fact that the sodium line emission is limited by the amount of exciter energy available, rather

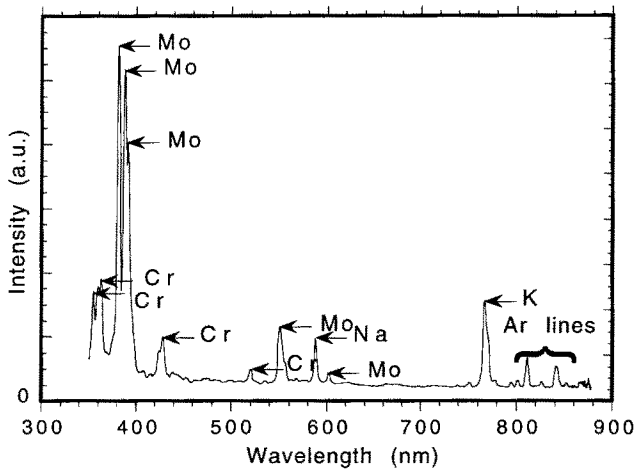

Fig. 3 Identification of the species responsible for the primary line emission observed at $x = 50$ mm, $y = 0$ mm

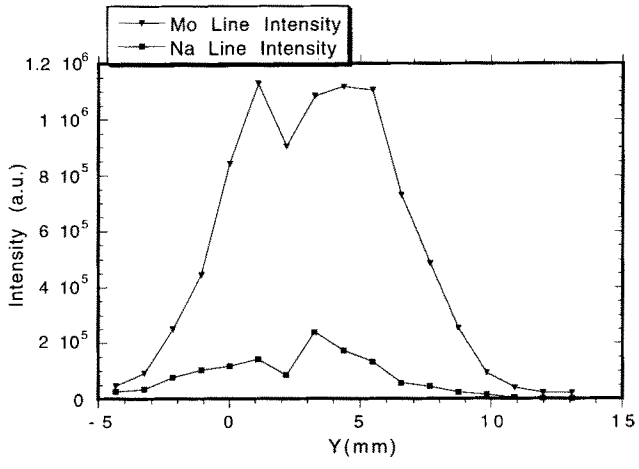

Fig. 4 Line intensities of the 380 nm Mo line and the 589 nm Na doublet as a function of y-position at $x = 50$ mm

than the amount of vapor present. Because the greater amount of excitation energy (both radiation and plasma kinetic energy) is nearer to the torch centerline, the sodium emission is strongest there. However, at $x = 140$ mm, the sodium emission changes from an exciter-energy limited state to a vapor-concentration limited state as evidenced by the line emission distribution closely paralleling the particle flux distribution. This transition to vapor-concentration limited emission is to be expected when vapor levels drop below a certain critical amount.

The difference in the line intensities of different elements is useful to bear in mind when analyzing particle temperature measurements. The line emission can act as a collected nonthermal signal along with the desired particle thermal signal. The thermal emission intensity for particles at a given temperature varies with the number of particles in the field of view. If the line emission intensity varies in proportion to the thermal emission intensity (or the particle flux), then the error induced in the calculated particle temperature by the line radiation is constant. Such would be the case for molybdenum vapor, because the line radiation intensity distribution closely follows the particle flux distribution. However, for the error induced in the calculated particle temperature by the sodium line radiation, the error is not independent of position. Closer to the centerline of the torch for $x = 80$ mm and $x = 110$ mm, the particle flux is low, but the sodium line intensity remains high. This causes the sodium line emission-induced temperature error to increase when moving from the particle plume centerline to the torch centerline.

As an illustration of the effect of line radiation on particle temperature measurements, consider the case of two-color pyrometry. As a worst possible case, assume that one of the spectral bands chosen for pyrometry includes the region of sodium line emission (589 nm). Assume that the other band chosen does not include any line emission (700 nm). Equation 1 is used to relate the ratio of intensities at two different wavelength bands to the surface temperature of the particles. For a gray-body material at 2880 K (the melting point of molybdenum), the ratio of thermal radiation intensities at 700 and 589 nm is 1.617. The strength of the sodium line emission compared to the particle thermal emission varies with y-position. Near the center of the particle plume ($y = 7.6$ mm) the sodium line causes a 3% increase in the signal at 589 nm. Near the torch centerline ($y = 3.3$ mm), the sodium line emission causes an 87% increase in the signal at 589 nm. The indicated particle temperatures which would result from a 3 and 87% increase in the intensity at 589 nm, with no increase in the intensity at 700 nm, would be 2945 K and 5389 K, respectively. Therefore, the particle temperatures measured by two-color pyrometry would be higher than the actual particle temperatures for this example. At the center of the particle plume, the temperature would be 2% higher, while the temperature near the torch centerline would be 87% higher. This indicates the temperature error introduced and how the error varies as a function of location in the plume. However, since it is unlikely that these exact spectral bands would be chosen for two-color pyrometry, errors actually encountered would be less than those illustrated here.

Vardelle et al. have made direct measurements of the density of vapor clouds that surround individual particles. They found that the vapor cloud spreads out to a distance of ~5 particle diameters (Ref 12). Eddy et al. have shown images of trails of vaporized particle material-emitting line radiation (Ref 13). These trails extended downstream from the particles and were 10 or more particle diameters in length. In the present study, the data indicate that the vapor signal for molybdenum is found only in

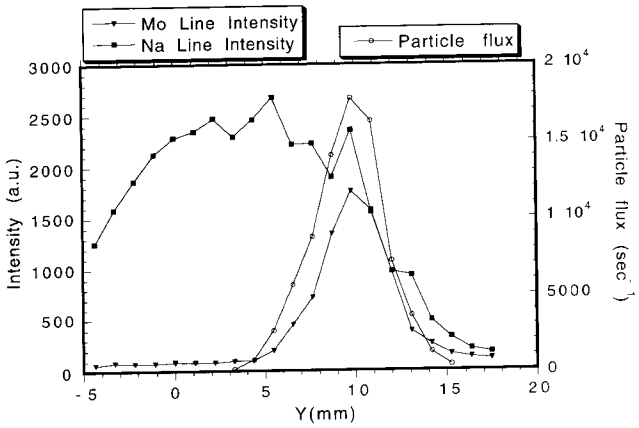

Fig. 6 Line intensities of the 380 nm Mo line and the 589 nm Na doublet, and the particle flux of hot Mo particles as a function of y-position at $x = 110$ mm

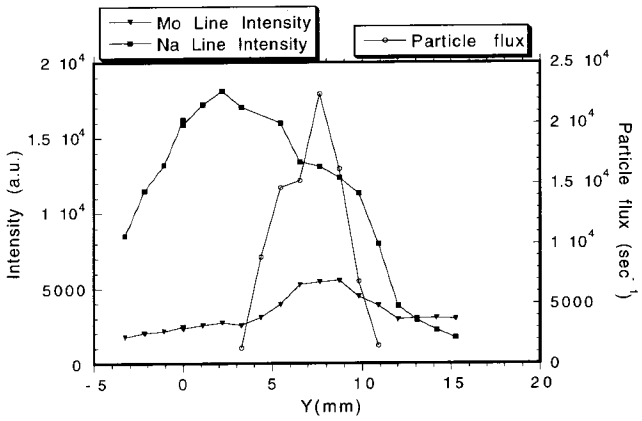

Fig. 5 Line intensities of the 380 nm Mo line and the 589 nm Na doublet, and the particle flux of hot Mo particles as a function of y-position at $x = 80$mm

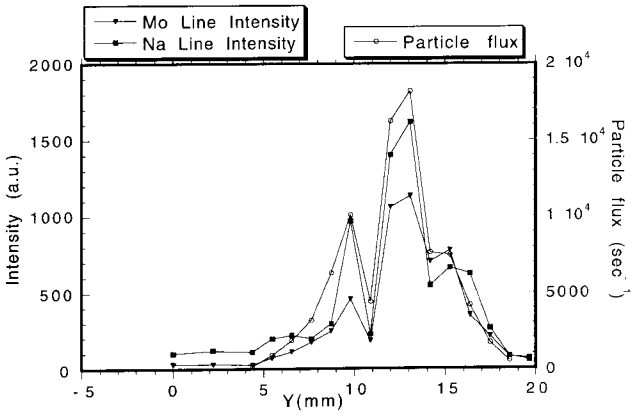

Fig. 7 Line intensities of the 380 nm Mo line and the 589 nm Na doublet, and the particle flux of hot Mo particles as a function of y-position at $x = 140$ mm

the vicinity of the particles. However, the vapor signal for sodium (as well as that for potassium as evidenced by its 766 nm emission line) remains strong even in regions where no particles are present. This means that the vapor forms an emitting cloud which extends well beyond particle trajectories. However, even though the vapor emission remains strong beyond particle trajectories, the vapor density may be very low.

4.3 Particle-Masking Effect

Because vapor radiation has been treated above and thermal radiation is covered in an accompanying paper (Ref 6), the next effects to be quantified are the particle effects. The first to be investigated is the particle-masking effect. One way to estimate this effect is to calculate the area fraction of the detector field of view that the particles comprise. At $x = 80$ mm, this was calculated using:

$$A_p = \frac{\pi}{4}(D_p)^2 \frac{n}{v \cdot \Delta y} \quad \text{(Eq 2)}$$

where A_p is the area fraction of particles in the field of view, D_p is the average particle diameter, v is the average particle velocity, n is the particle feed rate in units of number of particles/time, and Δy is the distance in the y-direction over which the particles

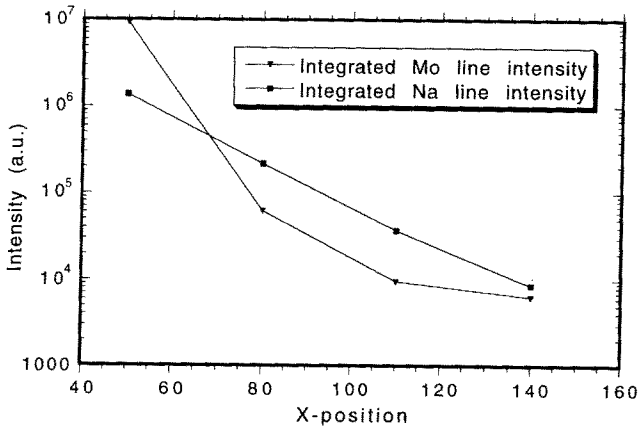

Fig. 8 Mo and Na line intensities integrated over all y-positions as a function of x-location

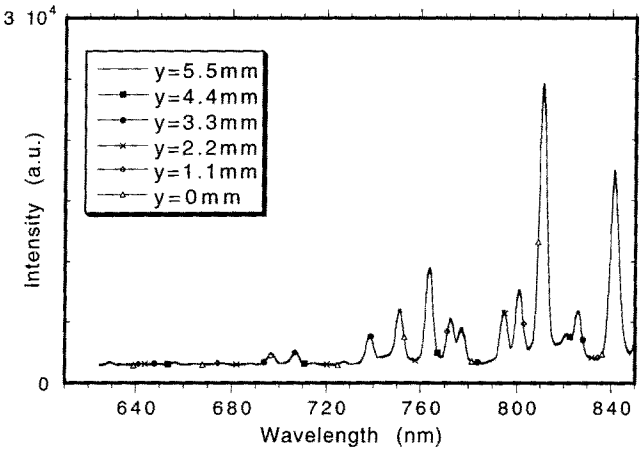

Fig. 9 Without-particle spectra at $x = 80$ mm

are spread at the chosen x-position. The average particle size is taken to be 69 μm as given by the center of the particle size distribution (narrow 63 to 75 μm size cut). The velocity of the particles was measured with laser two-focus velocimetry (L2F) to be 90 m/s at $x = 80$ mm, and Δy was found to be 8 mm from the hot particle flux distribution, as shown in Fig. 5. The average area fraction of the particles in the detector field of view at $x = 80$ mm was calculated from Eq 2 and the data given above to be 0.045%. The maximum area fraction of particles in the field of view occurs at the center of the particle plume where the particle flux is highest. At the center of the particle plume, the area fraction of particles in the field of view is 0.093%. With particles in less than 0.1% of the detector field of view, occasions of one particle masking the thermal emission signal from another particle are very rare. Blocking 0.1% of the plasma signal is likewise a very small effect. Furthermore, as the particles travel to higher x-values, they spread over a larger area causing an even smaller particle-masking effect. Thus, particle masking can be eliminated from further consideration in deconvoluting the signals present in the with-particle spectra because its effect is so small. However, this may not be the case for heavily particle-laden plasmas.

4.4 Spectral Plasma Loading Effect

Next, the spectral plasma loading effect (SPLE) of particles was quantified. In this analysis, the extent to which the intensity of a plasma line decreases due to the addition of particles is termed the SPLE. This effect can be investigated by observing the intensity of an argon plasma line before and after particles are added. There are two effects which change the line intensity upon the addition of particles to the plasma. One is the particle-reflected plasma light (PRPL) and the other is the SPLE. By observing the argon line intensity in a region through which no particles pass, there is no PRPL. In this type of region, the SPLE can be observed by itself.

Figure 9 shows the 630 to 880 nm without-particle signal for several y-locations at $x = 80$ mm. These signals are nearly identical in shape and intensity. This indicates that the without-particle signal is quite invariant with y-location. Figure 10 shows the with-particle spectra taken at the same locations. The increase in signal across the spectrum is primarily due to particle thermal emission. It can be seen that below $y = 2.2$ mm, the spectra are very similar in shape and intensity. This indicates that the thermal signals included in spectra with $y > 2.2$ mm are absent in the $y < 2.2$ mm spectra. Therefore, it can be concluded that because there is no thermal signal detected, there are no hot particles in the sampling volume at these y-locations. With-particle spectra that have no particles in the detector sampling volume will be referred to as "no-particle" spectra (as opposed to without-particle spectra where there is a complete absence of particles in the plasma). It is possible that there are some cold particles on the periphery of the plume, as have been observed by others (Ref 14-16). However, because the cold particles observed in Ref 14 to 16 consist primarily of very large or very small particles, and the particle-size distribution used for this experiment is very small (63 to 75 μm), it is expected that there are very few cold particles in the periphery of the plume.

In the no-particle region, because there is no PRPL, the intensity change of the plasma lines with the addition of particles

shows the SPLE. The 811 nm argon line was chosen for investigation because none of the species identified in the particle vapor signal have strong line emission in this region. For points in the no-particle region, the continuum-to-peak intensity for the 811 nm argon line in the with-particle spectrum and the corresponding line in the without-particle spectrum were compared. The 811 nm argon line intensity data for $x = 50$ mm is shown in Fig. 11, while that for $x = 80$ mm is in Fig. 12. The no-particle region for $x = 50$ mm is from $y = -6.5$ to 0 mm, and from $y = 9.8$ to 13.1 mm. The line intensities for the without-particle spectra were higher than for the corresponding with-particle spectra, indicating the presence of the SLPE. The amount of decrease in line intensity (or SPLE) was relatively constant at 9% for the data at $x = 50$ mm in the range from $y = -6.5$ to 0 mm. The SPLE in the range from $y = 9.8$ to 13.1 mm was a relatively constant 5%. The no-particle region for $x = 80$ mm is from $y = -4.4$ to 1.1 mm. The SPLE in this range was found to be ~3%. This indicates that there is a slight SPLE which decreases the plasma signal when the particles are added. The effect of the SPLE decreases for larger x-values and for locations further away from the plasma centerline. This seems reasonable, because further away from the plasma core, the temperature difference between the plasma and the particles is less, so there is less energy transferred from the plasma to the particles. At $x = 110$ mm and beyond (Fig. 13-15), the without-particle spectra line intensities at the edge of the particle plume are lower than the with-particle spectra line intensities indicating that there is no longer any no-particle region imaged. Therefore, there is no direct measure of the plasma loading effect for $x = 110$ mm and beyond.

Gougeon and Moreau (Ref 9) have observed a drop in the plasma intensity of 5 to 10% with a detector placed on the torch exit centerline upon the addition of 14 g/min of Ni particles to an argon plasma plume. This result seems generally consistent with the findings presented here. The head-on effects (as measured by Gougeon and Moreau) and side-on effects (as reported here) should not necessarily show the same result, as is the case for the comparison shown here.

4.5 Particle-Reflected Plasma Light

Next, the amount of plasma light reflection from particles was investigated. The amount of PRPL was determined by measuring the intensity of the 811 nm argon line above the continuum for with-particle and without-particle spectra. The intensity of the

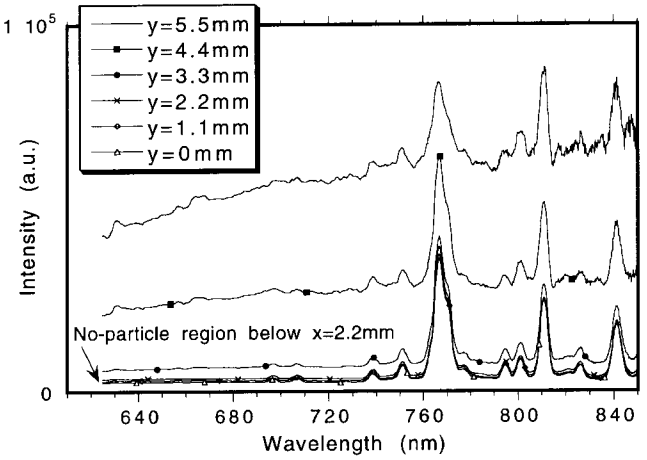

Fig. 10 With-particle spectra at $x = 80$ mm

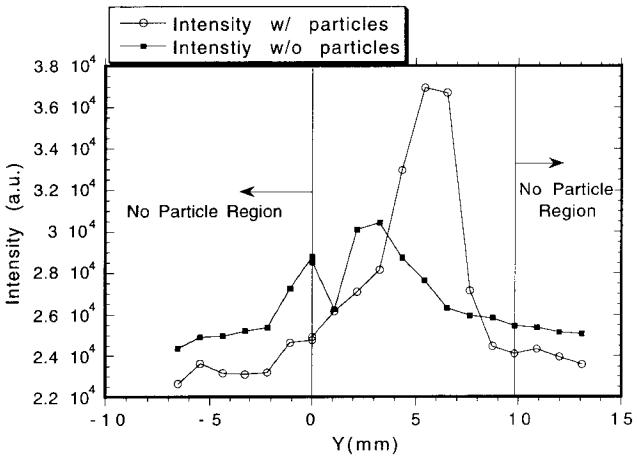

Fig. 11 With- and without-particle spectra: 811 nm Ar line height data at $x = 50$ mm

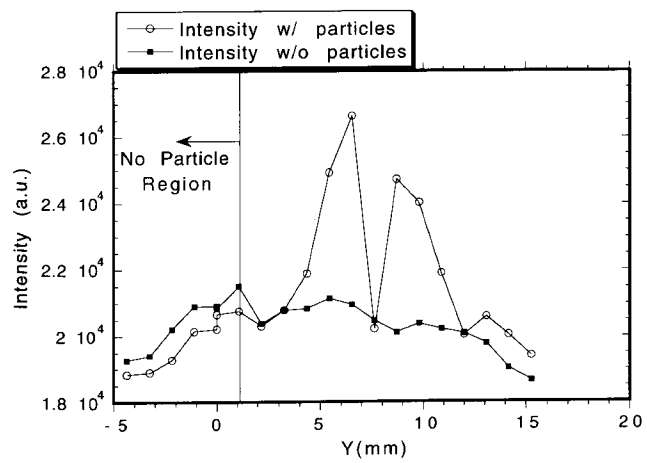

Fig. 12 With- and without-particle spectra: 811 nm Ar line height data at $x = 80$ mm

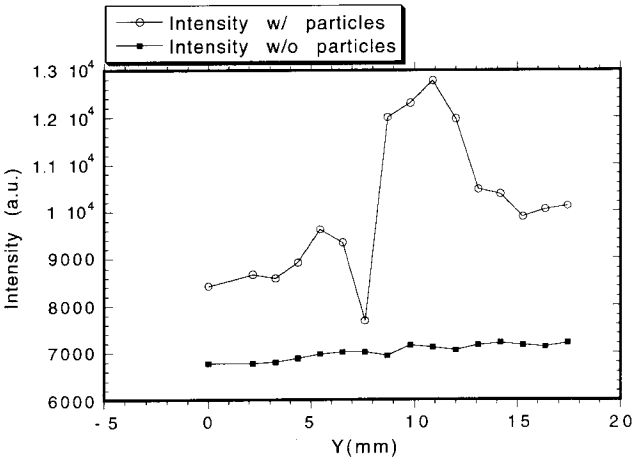

Fig. 13 With- and without-particle spectra: 811 nm Ar line height data at $x = 110$ mm

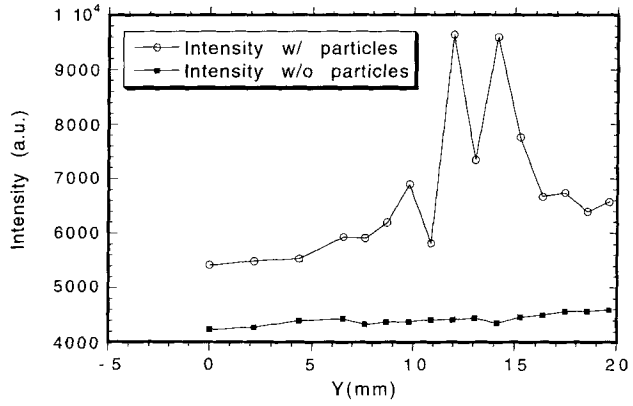

Fig. 14 With- and without-particle spectra: 811 nm Ar line height data at x = 140 mm

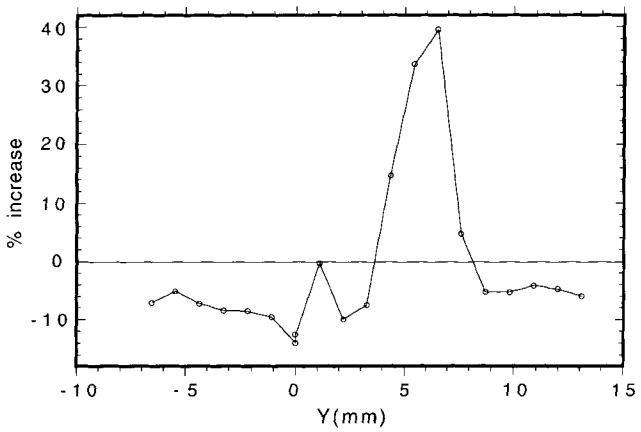

Fig. 16 Percent increase of the 811 nm Ar line intensity for spectra taken at x = 50 mm upon addition of particles

line in the with-particle spectra represents the plasma signal from around the particle plus the head-on plasma signal reflected by the particles into the detector. Note that the argon line spectra for the head-on signal and the without-particle signal are very similar in shape, even though the head-on spectrum is much higher in intensity. The measurements for determining the PRPL were made in regions where particles are in the detector field of view.

The change in line height of the 811 nm Ar line upon the addition of particles represents a combination of the SPLE and the PRPL signals. The SPLE has been quantified previously to be about 10% or less for x-positions of 50 mm and greater. With an estimate of the SPLE, the total change in line height can be used to calculate the PRPL signal. Figure 16 shows the percent increase in the 811 nm Ar line intensity at x = 50 mm upon the addition of particles to the plasma. The particle plume in the y = 3.5 to 8 mm region causes an increase in line height due to the PRPL signal. The maximum intensity change due to the SPLE and the PRPL at x = 80 mm is a 40% increase in line height at y = 6.5 mm. Because the SPLE accounts for a 9% decrease in line intensity below the particle plume ($x \leq 0$ mm) and a 5% decrease in line intensity above the particle plume ($x \geq 9.8$ mm), a reasonable estimate for the SPLE at the center of the particle plume would be 7%. To determine the PRPL, the loss in line intensity due to the SPLE must be added to the line intensities from Fig.

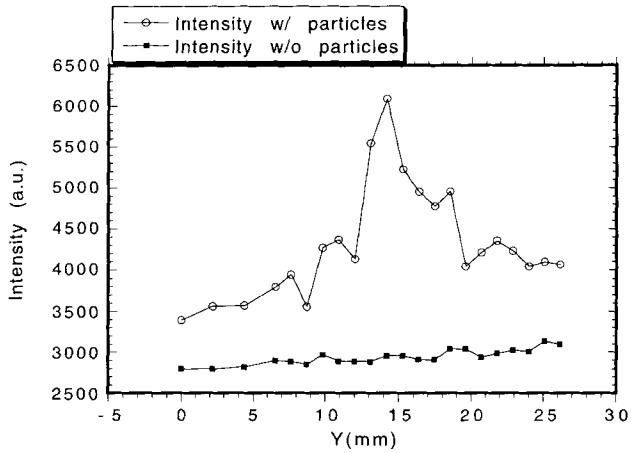

Fig. 15 With- and without-particle spectra: 811 nm Ar line height data at x = 170 mm

16 to give the total PRPL. Therefore, the PRPL at y = 6.5 mm causes a 47% increase in the argon line intensity. Figure 16 shows how the SPLE dominates at the edges of the particle plume, while the PRPL dominates near the center of the particle plume (negative and positive line intensity increase regions, respectively). The two effects approximately offset each other in the intermediate particle flux regions. The effect of PRPL can be seen in Fig. 12 to 15 for x = 80 to 170 mm. The increase in line intensity corresponds to the location of the particle plume; for the x = 110 to 170 mm region, it is as high as 120%. This increase in the PRPL with distance from the torch exit results from the without-particle plasma signal dropping faster with increasing x-location than the head-on plasma signal (which is the source of the PRPL signal). The data show that particle-reflected light causes a significant increase in the nonthermal emission component of the with-particle signal for all x-positions. Therefore, proper attention should be paid to this effect when collecting spectra for particle temperature measurements in order to minimize temperature error induced by the nonthermal emission signal.

5. Conclusions

The spectral analysis of the nonthermal emission signal of a molybdenum particle-laden plasma torch plume has yielded the following results:

- Species in the plasma plume were identified from their characteristic emission lines. In addition to the lines expected from the Ar plasma and the Mo particle vapor, Cr, Na, and K lines were observed. This indicates that emission from powder impurities can be a significant source of nonthermal radiation in the plasma/particle plume. In calculating particle surface temperatures, care must be exercised to compensate for the plasma, powder, and impurity line radiation present, unless it is known for certain that no lines exist in the spectral region sampled. In addition to the line emission, there is some amount of continuum radiation emitted from the plasma and vapor species present, which must also be compensated for in calculating particle temperatures.

- For x-distances of less than 140 mm, the molybdenum emission lines are vapor-concentration limited, whereas the sodium emission lines appear to be exciter-energy limited. For x = 140 mm and beyond, line emission for both vapors are concentration-limited. Concentration-limited emission causes a relatively constant error in particle temperature measurements because the line emission intensity varies in the same manner as the thermal emission intensity. However, for exciter-energy limited emission, the particle temperature error increases when moving from the particle trajectory centerline to the plasma centerline for a given x-distance. This indicates the need for understanding of the different types of vapor line emission signals present in the spectral range used for particle temperature measurements, in order to properly treat the temperature uncertainties involved.
- Particle masking in a lightly particle-laden plume, as used in this study, has no significant effect on the thermal or nonthermal emission signals present in spectral data used for particle surface temperature measurements.
- The spectral plasma loading effect (SPLE) that causes a decrease in the plasma emission signal was measured to be in the range of 3 to 9% for x-distances of 50 and 80 mm. The extent of the SPLE decreases for larger x-values and for locations further away from the plasma centerline.
- The PRPL was found to significantly increase the argon line intensity detected. Values for increases in the argon line intensity, found to be as high as 120%, indicate the need to pay proper attention to this effect when collecting spectra for particle temperature measurements.

Acknowledgments

This research was performed under appointment to the Magnetic Fusion Energy Technology Fellowship program administered by Oak Ridge Institute for Science and Education for the U.S. Department of Energy. This work was performed at Sandia National Laboratories, operated by Lockheed Martin for the U.S. Department of Energy under contract DE-AC04-94AL85000.

References

1. M. Vardelle, A. Vardelle, A.C. Leger, and P. Fauchais, Dynamics of Splat Formation and Solidification in Thermal Spraying Process, *Thermal Spray Industrial Applications,* C.C. Berndt and S. Sampath, Ed., ASM International, 1994, p 555-562
2. R. McPherson, A Review of Microstructure and Properties of Plasma Sprayed Ceramic Coatings, *Surf. Coat. Technol.,* Vol 39 (No.40), 1989, p 173-181
3. J. Mishin, M. Vardelle, J. Lesinski, and P. Fauchais, Two-Colour Pyrometer for the Statistical Measurement of the Surface Temperature of Particles Under Thermal Plasma Conditions, *J. Phys. E, Sci. Instrum.,* Vol 20, 1987, p 620-625
4. S. Kuroda, T. Fukushima, S. Kitahara, H. Fujimori, Y. Tomita, and T. Horiuchi, Monitoring of Thermally Sprayed Particles Using Thermal Radiation, Vol 2, Paper 27 of *Proc. of 12th Int. Conf. on Thermal Spraying,* I.A. Bucklow, Ed., The Welding Institute, Cambridge, UK, 1989
5. J.R. Fincke, W.D. Swank, and C.L. Jeffery, Simultaneous Measurement of Particle Size, Velocity, and Temperature in Thermal Plasmas, *IEEE Trans. on Plasma Sci.,* Vol 18 (No. 6), 1990, p 948-957
6. K.J. Hollis and R.A. Neiser, Particle Temperature and Flux Measurement Utilizing a Nonthermal Signal Correction Process, *J. Therm. Spray Technol.,* Vol 7 (No. 2), p 392-402
7. K.J. Hollis and R.A. Neiser, Spectral Analysis of a Molybdenum Particle Laden Plasma Plume, *Advances in Thermal Spray Science & Technology,* C.C. Berndt and S. Sampath, Eds., ASM International, 1995, p 129-134
8. T. Sakuta and M.I. Boulos, Novel Approach for Particle Velocity and Size Measurement Under Plasma Conditions, *Rev. Sci. Instrum.,* Vol 59 (No. 2), 1988, p 285-291
9. P. Gougeon and C. Moreau, In-Flight Particle Surface Temperature Measurements: Influence of the Plasma Light Scattered by the Particles, *Thermal Spray Coatings: Research, Design and Applications,* C. C. Berndt and T.F. Bernecki, Ed., ASM International, 1993, p 13-18
10. J. Prucha and Z. Skarda, The Improvement of the Spectroscopical Temperature Diagnostic of Plasma Sprayed Particles, *Thermal Spray: International Advances in Coatings Technology,* C.C. Berndt, Ed., ASM International, 1992, p 343-348
11. A.N. Zaidel', V.K. Prokof'ev, S.M. Raiskii, V.A. Slavnyi, and E.Ya. Shreider, *Tables of Spectral Lines,* IFI/Plenum, 1970 (in Russian)
12. M. Vardelle, C. Trassy, A. Vardelle, and P. Fauchais, Experimental Investigation of Powder Vaporization in Thermal Plasma Jets, *Plasma Chemistry and Plasma Processing,* Vol 11 (No. 2), 1991, p 185-201
13. T.L. Eddy, B.A. Detering, and G.C. Wilson, LTE and Non-LTE Gas Temperatures in Loaded and Unloaded Plasma During Spraying of NiAl Powders, *Thermal Spray Research and Applications,* T.F. Bernecki, Ed., ASM International, 1990, p 33-37
14. R.A. Neiser and T.J. Roemer, An Investigation of Particle Trajectories and Melting in an Air Plasma Sprayed Zirconia, *Thermal Spray: Practical Solutions for Engineering Problems,* C.C. Berndt, Ed., ASM International, 1996, p 285-293
15. K.I. Lee, M. Vardelle, A. Vardelle, P. Fauchais, and C. Trassy, Vaporization of Metal Powders in Plasma Sprays, *Thermal Spray: Practical Solutions for Engineering Problems,* C.C. Berndt, Ed., ASM International, 1996, p 547-552
16. J.R. Fincke and W.D. Swank, The Effect of Plasma Jet Fluctuations on Particle Time-Temperature Histories, *Thermal Spray Coatings: Properties, Processes and Applications,* T. F. Bernecki, Ed., ASM International, 1991, p 193-198